Orbital Period Variation in the Chromospherically Active Binary FF UMa (2RE J0933+624)

M.C. Gálvez[1,2], D. Montes[2], M.J. Fernández-Figueroa[2], E. De Castro[2] & M. Cornide[2]

[1] Department of Astronomy, University of Florida, Bryant Space Science Center, Gainesville, Florida, USA
[2] Dept. de Astrofísica, Facultad de Físicas, Universidad Complutense de Madrid, Madrid, Spain

IAU Symp. 240:
Binary Stars as Critical Tools & Tests in Contemporary Astrophysics

Abstract

We present here a detailed study of FF UMa (2RE J0933+624), a recently discovered, X-ray/EUV selected, active binary system with strong Ha emission. By using high resolution echelle spectroscopic observations taken during five observing runs from 1998 to 2004, we derived precise radial velocities that allowed us to determine the orbital solution of the system at different epochs. Analyzing these orbital solutions and a previous one in 1993, determined by other authors, we have found a change in the heliocentric Julian date on conjunction (T_{conj}) that can be explained by a change with time in the orbital period of the system. The relative amplitude of the orbital period variation derived from these data was dP/P ~ 5 x 10-4, which results to be larger than the variations found in other similar chromospherically active binaries like AR Lac an HR 1099. This orbital period variation can be related (Applegate 1992; Lanza et al. 1998, 2006) with the modulation of the gravitational quadrupole-moment of its magnetically active secondary star produced by angular momentum exchanges within its convective envelope. In addition, using these observations, we have determined the stellar parameters of the components and we have carried out a study of the chromospheric activity using all the optical indicators from Ca II H & K to Ca II IRT lines.

Observations

The spectroscopic observations of this binary system were obtained during five observing runs from 1998 to 2004:

1) 12 to 21 January 1998 using the 2.1m Otto Struve Telescope at McDonald Observatory Texas (USA) with the Sandiford Cassegrain Echelle Spectrometer. During this observing run, a 1200x400 pixel CCD detector was used. The spectrograph setup was chosen to cover the Ha (6563 Å) and Ca II IRT (8498, 8542, 8662 Å) lines. The wavelength range covers from 6400 to 8800 Å in 31 orders. The reciprocal dispersion ranges from 0.06 to 0.08 Å /pixel and the spectral resolution, determined as the FWHM of the arc comparison lines, ranges from 0.13 to 0.20 Å. In one of the nights, we changed the spectrograph setup to include the He I D_3 (5876 Å) and Na D_1, D_2 (5889.9, 5895.9 Å), with wavelength coverage of 5600-7000 Å.

2) 22 to 24 January 2000 using the 9.2m Hobby-Eberly Telescope (HET) at McDonald Observatory Texas (USA), with the medium resolution spectrograph UFOE (Upgraded Fiber Optic Echelle). A 1200x400 pixel CCD detector was used.The wavelength range covers from 4400-9150 Å in 26 orders. The reciprocal dispersion ranges from 0.06 to 0.17 Å/pixel and the spectral resolution (FWHM) from 0.14 to 0.42 Å.

3) and ***4)*** April 2002 and April 2004. These observing runs took place on 22 to 26 April 2002 and from 29 March to 7 April 2004, using the 2.2m telescope at the German Spanish Astronomical Observatory (CAHA) (Almeria, Spain). The Fibre Optics Cassegrain Echelle Spectrograph (FOCES) was used with a 2048^2 24µ and 150µ respectively SITE#1d15 CCD detector. The wavelength range covers from 3450 to 10700 Å in 112 orders. The reciprocal dispersion ranges from 0.04 to 0.13 Å/pixel and the spectral resolution (FWHM) ranges from 0.08 to 0.35 Å.

5) This run were made on 2 to 6 April 2004, using the 2.56m Nordic Optical Telescope (NOT) located at the Observatory Roque de Los Muchachos (La Palma, Spain). The Soviet Finnish High Resolution Echelle Spectrograph (SOFIN) was used with an echelle grating (79 grooves/mm), ASTROMED-3200 camera and a 2052^2 pixel 2K3EB PISKUNOV1 CCD detector. The wavelength range covered is from 3545 to 10120 Å in 42 orders. The reciprocal dispersion ranges from 0.033 to 0.11 Å/pixel and the spectral resolution (FWHM) from 0.14 to 0.32 Å.

Radial Velocities

Heliocentric radial velocities of both components have been determined by using the cross-correlation technique. The spectra of the program stars were cross-correlated order by order, using the routine FXCOR in IRAF, against spectra of radial velocity standards of similar spectral types. The velocity is derived from the position of the cross-correlation peak (Fig. 1 A and B). In Table 1 we list the final obtained heliocentric radial velocities (V_{hel}) and their associated errors (σ_V) for each spectrum. As the system is SB2 we can see two peaks in the CCF coming from the two components and we can fit each peak separately. When the components are too close, we used deblend fits. But as it can be seen in the Fig. 1A the irregulars profiles (double peaks and asymmetries) can produce errors in radial velocity measures. To correct this error, we recalculated the radial velocities using the cross-correlation technique against spectra of the same radial velocity standard star but rotational broadened to the rotational velocity of the components of FF UMa ($v\sin i$ ~30 km s^{-1}). This way the profiles of CCF become regulars, see Fig. 1B.

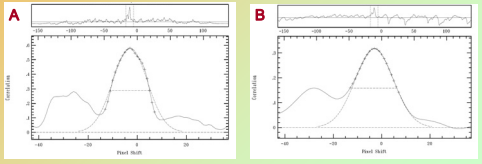

Fig. 1: Cross-correlation functions (CCFs) of the both components of the binary system, fitted with Gaussians. **A)** left panel, original CCF, **B)** right panel, corrected CCF.

References

1. Applegate J.H., 1992, ApJ, 365, 621
2. Barden S.C., 1985, ApJ, 295, 162
3. Cumming A., 2004, MNRAS, 354, 1165
4. Frasca A. & Lanza A.F., 2005, 429, 309
5. Jeffries R.D., Bertram D & Spurgeon R.D., 1995, MNRAS, 276, 397
6. Lanza A.F., Rodono. M & Rosner R., 1998, MNRAS, 296, 893
7. Lanza A.F., 2006, MNRAS, 369, 1773L
8. Matese J.J. & Whirtmere D.P., 1983, A&A, 117, L7
9. Montes D., Fernández-Figueroa M.J., De Castro E. & Cornide M.,1995, A&A, 294, 165
10. Montes D., Fernández-Figueroa M.J., De Castro E. & Sanz-Forcada J.,1997, A&A, 125, 263
11. Montes D., Sanz-Forcada J., Fernandez-Figueroa M.J., De Castro E. & Poncet A., 1998, A&A, 330, 155

Orbital Solution

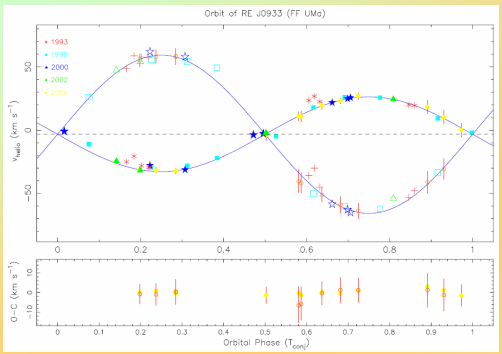

Fig. 2: Radial velocities of all observing runs. We plotted the orbital solution (continuum line) of the FOCES04 observing run and we have superimposed the data from the rest runs shifted in phase according with the determined O-C in T_{conj} see tex for explanation. Different symbols and colours correspond to different epochs (1993 (Jeffries et al. 1995), and 1998 - 2004 our observing runs).

Table 1: Radial velocity data of the 5 observing runs and data taken from previous authors.

Obs.	MJD 2400000+	S/N (Hα)	Primary $V_{hel} \pm \sigma_V$ (km s^{-1})	Secondary $V_{hel} \pm \sigma_V$ (km s^{-1})
Jef(95)[1]	49054.591	-	23.5 ± 4.0	-38.9 ± 9.0
Jef(95)[1]	49054.634	-	26.5 ± 3.0	-30.0 ± 9.0
Jef(95)[1]	49054.675	-	22.6 ± 3.0	-45.0 ± 5.0
Jef(95)[1]	49055.375	-	20.0 ± 3.0	-53.3 ± 3.0
Jef(95)[1]	49055.425	-	19.5 ± 3.0	-47.6 ± 4.0
Jef(95)[1]	49056.425	-	-25.1 ± 5.0	48.7 ± 3.0
Jef(95)[1]	49056.486	-	-20.6 ± 4.0	58.8 ± 3.0
Jef(95)[1]	49056.543	-	-28.1 ± 4.0	57.8 ± 3.0
Jef(95)[1]	49056.600	-	-29.4 ± 4.0	57.3 ± 3.0
MCD98	50826.935	146	25.80 ± 1.92	-62.05 ± 4.75
MCD98	50827.915	205	-11.09 ± 2.26	36.23 ± 5.92
MCD98	50828.922	98	-22.16 ± 1.71	49.39 ± 4.58
MCD98	50829.929	139	25.95 ± 1.86	-60.06 ± 4.29
MCD98	50830.932	95	-1.88 ± 3.50	-
MCD98	50831.961	134	-28.27 ± 1.72	54.33 ± 4.59
MCD98	50832.958	146	17.89 ± 1.63	-50.03 ± 6.42
MCD98	50833.935	83	9.94 ± 4.51	-33.82 ± 4.72
MCD98	50834.953	77	-29.42 ± 1.78	55.83 ± 4.90
MCD98	50836.039	115	-4.99 ± 6.29	-
HET00	51561.945	- *	-27.96 ± 2.60	61.98 ± 2.80
HET00	51562.759	233	-3.74 ± 6.51	-
HET00	51562.837	- *	-2.75 ± 6.50	-
HET00	51566.774	263	24.78 ± 2.66	-62.86 ± 2.81
HET00	51566.797	- *	25.66 ± 2.66	-65.02 ± 2.81
HET00	51567.812	83	-0.97 ± 6.21	-
HET00	51568.767	146	-31.61 ± 2.29	58.01 ± 2.70
HET00	51569.925	236	21.76 ± 2.64	-58.45 ± 2.53
FOCES02	52387.329	118	-31.89 ± 2.33	54.19 ± 4.49
FOCES02	52388.320	200	-2.24 ± 4.13	-
FOCES02	52389.323	140	24.44 ± 2.56	-54.03 ± 4.62
FOCES02	52390.414	146	-24.46 ± 2.63	47.54 ± 4.93
FOCES04	53096.4836	71	26.98 ± 2.58	-63.76 ± 6.27
FOCES04	53098.5186	65	-32.32 ± 2.66	58.08 ± 6.46
FOCES04	53099.5077	87	10.94 ± 3.24	-41.79 ± 8.17
FOCES04	53099.4756	74	19.50 ± 2.98	-51.18 ± 5.88
FOCES04	53099.6158	59	23.20 ± 2.31	-58.85 ± 6.54
FOCES04	53100.5048	98	18.38 ± 4.44	-41.51 ± 8.71
FOCES04	53100.4329	117	10.31 ± 4.15	-30.65 ± 8.26
FOCES04	53100.5718	80	0.24 ± 4.41	-
FOCES04	53101.3082	86	-31.11 ± 2.05	55.25 ± 5.04
FOCES04	53101.4374	122	-31.93 ± 2.44	58.35 ± 5.54
FOCES04	53101.5952	150	-32.02 ± 2.18	58.24 ± 5.44
FOCES04	53102.3061	117	-3.95 ± 4.25	-
FOCES04	53102.5640	95	13.02 ± 3.46	-40.59 ± 8.89
NOT04a[2]	53098.4155	225	-22.98 ± 1.20	68.66 ± 4.50
NOT04a[2]	53098.4268	150	-22.99 ± 1.25	-67.88 ± 4.49
NOT04a[2]	53099.5426	243	61.79 ± 1.17	-21.23 ± 4.36
NOT04a[2]	53101.4019	227	-19.89 ± 1.30	79.70 ± 3.54

[1] JEF(95): Jeffries et al. (1995)
[2] Values not taken into account in orbital solution calculation.

Table 2: Orbital solution of FF UMa. All the parameters are calculated for the observing run that we take as a reference (FOCES04). The orbit results circular. With the resulting parameters and assuming a secondary star spectral type (**K0V**) from the spectrum, we estimated the mass and a minimum radium of the primary as **1.67 $M_\odot$** and **2.17 $R_\odot$** in agreement with our **subgiant** classification.

Element	Value	Uncertainty	Units
P_{orb}	3.2735	0.0537	days
T_{Conj}	55090.8398	0.1753	HJD (2400000 +)
ω	0.0000	0.0000	degrees
e	0.0000	0.0000	(adopted)
K_1	29.5520	0.9479	km s^{-1}
K_2	62.5166	3.6018	km s^{-1}
γ	-3.2324	0.7716	km s^{-1}
$q = M_1/M_2$	2.1155	0.1012	
$a_1 \sin i$	1.3303	0.0479	10^6 km
$a_2 \sin i$	2.8141	0.1686	10^6 km
$a \sin i$	4.1444	0.1753	10^6 km
a	0.02770		AU
a	5.9546		$R_\odot$
$M_1 \sin^3 i$	0.1797	0.0239	$M_\odot$
$M_2 \sin^3 i$	0.0850	0.0118	$M_\odot$
$f(M)$	0.0087534	0.0009888	$M_\odot$

Orbital Period Variation

With 39 radial determined by us (from 1998 to 2004) and 9 given by Jeffries et al. (1995), we tried to compute the orbital solution but we find some tricking facts. When we fit the data from each observing run separately we obtain a good orbital solution, but when we tried to fit the total orbital solution (using all the radial velocities from the different epochs) we are not able to find a good orbital solution. Analyzing in detail these results we discover that orbital parameters obtained at different epochs are very similar, but there is a shift in the heliocentric Julian date on conjunction (T_{conj}). See Fig. 2 and 3.
Taken this into account, we computed the orbital solution with the FOCES04 run and shifted in phase the rest of the observing runs. See the orbital solution section.

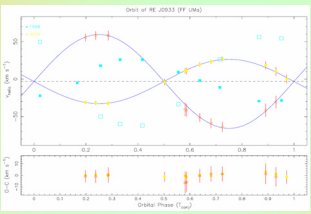

Fig. 3: Note the orbital phase shift between the orbital solutions obtained with the data of the FOCES04 observing run (continuum line) and McDonald 1998 (blue squares).

We have analyzed the different hypothesis that can explain this behaviour :

1. The existence of another star as a distant third component of the system could introduce changes in the main orbit of the observed system. Variations in in the center of mass radial velocity (γ) could indicate the presence of a third component (Cumming 2004). However, the amplitude of the variations in γ we have found in our data is only of 3 km s^{-1}.

2. The presence of photospheric starspots in the active components of this binary, could produce asymmetries in the absorption line profiles and the corresponding CCF. This could affect the radial velocity data and this way transmit errors to the orbital solutions. However, we have found (see radial velocities section) that this is not the case.

3. Another explanation associated to the magnetic activity could be an orbital period modulation due to the variation of activity with time. It can be explained as a consequence of *cyclic variations of the quadrupole-moment of both components of the system along the magnetic activity cycle*. In the study of the RS CVn system HR 1099, Frasca & Lanza (2005) based on the hypothesis presented by Matese & Whirtmere (1983) and elaborated later by Applegate (1992) and Lanza et al. (1998), in which temporal variations of some RS CVn systems could be due to changes in the quadrupole-moment of primary component along the activity cycle and that come from the exchange between kinematics and magnetic energy driven by the stellar hydromantic dynamo.
The results obtained until this study were variations of dP/P~10^{-6}-10^{-5} in an interval of 7 to 109 years. In FF UMa we have found a variation of *dP/P~10^{-4} in 11 years*, one order of magnitude higher, but it could be explained by the higher efficiency of the dynamo mechanism in the components of the system.

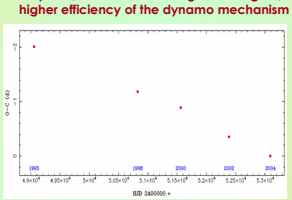

Year	TConj HJD (2400000 +)	O-C day	dP/P
1993	49055.8789	-2.0089	4.979x10-4
1998	50824.4023	-1.1755	5.187x10-4
2000	51561.2227	-0.9005	5.887x10-4
2002	52386.6758	-0.3615	5.134x10-4
2004	53090.8398		

Fig. 4 and Table 3: T_{conj} shift (O-C) at the different epochs and the derived orbital period variation.

In Table 3 we present the orbital period variation deduced from the orbital solution of the different observing runs, in the first column we give the year of the observing run, in the second, T_{conj} in the third, the O-C (Observed – Calculated = difference between the observed T_{conj} and calculated T_{conj} from the FOCES04 run that has been taken as reference), and in the last column the relative orbital period variation. dP/P. Fig. 4. represents the variation of the O-C (T_{conj}) for every run with time. The amplitude of the variation is 2 days and it look like a linear tendency. We would need a larger time observation for testing if the tendency remains linear of becomes sinusoidal as it is expected if there is a cycled motion.

Although recent studies, as Lanza (2006), are not completely in agreement with Applegate model, we found that the quantitative explanation of the phenomena is the most likely for FF UMa system.

Chromospheric activity

The chromospheric contribution in the different optical chromospheric activity indicators has been determined using the spectral subtraction technique Montes et al. (1995; 1997; 1998). The synthesized spectrum was constructed using the program STARMOD developed at Penn State (Barden 1985). In Table 4, we give the excess emission absolute superficial flux ($\log F_j$) (measured in the subtracted spectra) for these lines. We have deblended the emission from both components using a two-Gaussian fit except for *Hα*. The profiles of the Hα, and Ca II IRT (λ8498, λ8542) lines are plotted in Figs. 5 and 6. For each observation we have plotted the observed spectrum (solid-line) and the synthesized spectrum (dashed-line) in the left panel and the subtracted spectrum (dotted line) in the right panel.
Hα line is observed always in emission above the continuum in the observed spectra for both components, (see Fig. 5). This emission is persistent during all the observations indicating that it is a very active binary system similar to some RS CVn and BY Dra systems.

Fig. 5: Hα | **Fig. 6: Ca II IRT**

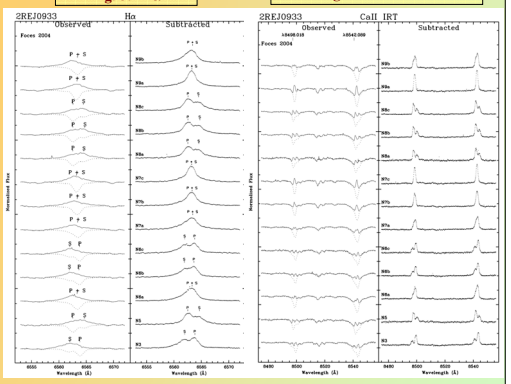

Measuring EW of this line, we found that each star of the system have a wide component that avoid to fit the emission lines with one Gaussian. Due to we either could not fit the emission lines with four components (two, narrow and wide components, for each star), we found that the best fits was a *Lorentzian* curve, one for each component (see Fig.7). Absorption of the three, Hβ, Hγ and Hδ lines filled in with emission is seen too (see Fig. 8 for Hβ example) as Has well as a stronge mission in the Ca II H & K lines and a clear emission in the *Hε* line coming from both components. As is represented in fig 6 a clear emission above the continuum is observed in the core of the Ca II IRT absorption lines from both components.

Fig. 8: Hβ

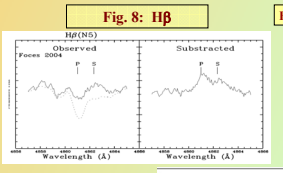

Fig. 7: Lorentzian fitting of Hα profile.

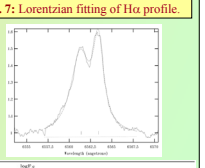
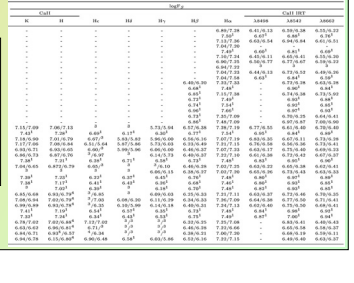
Table 4:
Absolute superficial flux of all the activity indicators.
1. Value of the primary and secondary not deblended.
2. Average value from two apertures.
3. Value measured with low S/N.
4. Ca II H line from one component blended with Hε line from the other component.